PHOTONICS Research

Distributed static and dynamic detection of an acoustic wave in a Brillouin random fiber laser

Zichao Zhou,* Haiyang Wang, Yuan Wang, Liang Chen, and Xiaoyi Bao

Department of Physics, University of Ottawa, Ottawa, Ontario K1N 6N5, Canada
**Corresponding author: zzhou030@uottawa.ca*

Received 23 November 2020; revised 8 February 2021; accepted 1 March 2021; posted 3 March 2021 (Doc. ID 415747); published 26 April 2021

The interaction of random laser and gain medium is important to understand the noise origin in random fiber lasers. Here, using the optical time domain reflectometry method, the time-resolved distributed acoustic wave generated by a Brillouin random fiber laser (BRFL) is characterized. The dynamic property of the acoustic wave reflects the gain dynamics of the BRFL. The principle is based on the polarization-decoupled stimulated Brillouin scattering (SBS)-enhanced four-wave mixing process, where the probe light experiences maximum reflection when the phase match condition is satisfied. Static measurements present exponentially depleted Brillouin gain along the gain medium in the BRFL, indicating the localized random SBS frequency change in the maximum local gain region, which varies with time to contribute random laser noise as revealed in the dynamic measurement. The SBS-induced birefringence change in the Brillouin gain fiber is approximately 10^{-7} to 10^{-6}. The phase noise of the BRFL is observed directly inside the random laser gain medium for the first time via time and spatially varied acoustic wave intensity. By counting the temporal intensity statistical distribution, optical rogue waves are detected near the lasing threshold of the BRFL. Different temporal intensity statistical distribution at high and low gain positions is found, which is caused by the SBS nonlinear transfer function and localized gain. The distributed characterization methods in the paper provide a new platform to study the interaction of random lasers and gain medium, giving us a new perspective to understand the fundamental physics of the random lasing process and its noise property.

https://doi.org/10.1364/PRJ.415747

1. INTRODUCTION

Random fiber lasers have recently attracted a great deal of attention due to their novel underlying physics and great potential applications [1–5]. Different from the conventional lasers that require a cavity with a fixed length to trap light, random fiber lasers make use of the multiple scattering of photons in a disordered medium to provide optical feedback. Lasing occurs when the total gain in the random cavity overcomes the total loss. The characteristics of random lasers are determined by the radiation buildup by multiple scattering of the disordered medium and the light amplifying process in the gain medium, resulting in versatile unique output properties in different random fiber laser schemes. The first demonstration of the random fiber laser was based on random nanoparticles scattering in colloidal suspension inserted in the hollow-core fiber [6], which was then followed by the realization of the coherent random fiber laser in a similar configuration [7]. Recent research found the statistical turbulence signatures in the distribution of intensity fluctuations in a continuous wave pumped erbium-based random fiber laser with random Bragg grating scatters [8,9], which provide a platform to study the challenging turbulent behavior in photonics. Replica symmetry breaking was demonstrated in random fiber lasers, where the transition from a photonic paramagnetic to a photonic spin-glass phase was verified and indicated the glassy random fiber laser behavior [10]. Near lasing threshold, the statistical distribution of the random fiber laser was characterized by a power law tailed function consistent with a Lévy α-stable distribution as a universal existence of such statistical properties in random lasing systems [11,12]. The simple architecture of the random fiber laser has provided a perfect photonics platform to study the fundamental physics in various random systems. Since there is no need to form a precise microcavity, the production cost of the random fiber laser is low, which makes great potential applications in fiber sensing [13–15] and low-noise fiber lasers [16–19]. However, for many applications, the current performance of the random fiber laser has to be improved, especially due to its large intensity noise [20,21]. Different from the conventional fiber lasers, a large number of random modes are formed in random fiber lasers, making it difficult to describe their dynamic process. Though wave kinetic theory was developed to describe the random lasers with a large number of generation modes [22], the fundamental physics behind random fiber lasers remains unclear in many phenomena, such as the

Lévy statistics [23,24], spectral correlations [25], and optical rogue waves [26] in random fiber lasers. Stimulated Brillouin scattering (SBS) is a major noise source in various random fiber laser systems, especially with Raman gain medium-based random laser, which has a higher threshold than the SBS threshold. The stochastic behavior of the random fiber laser originated from SBS process was studied in a random fiber laser based on Raman gain recently [27]. At the same time, SBS can be utilized as the gain mechanism to build the random fiber laser [28,29], which provides a good platform to study the noise characteristic of the SBS process enhanced by the multiple scattering in disordered media. The intrinsic spectral width and intensity dynamics of the acoustic wave in a polarized Brillouin random fiber laser were characterized experimentally [30]. The characterization mechanism was based on the polarization-dependent central wavelength of the acoustic-wave-induced dynamic grating, which was similar to the population-inversion-based dynamic grating in an open-cavity Yb-doped fiber laser with distributed feedback [31]. However, the distributed spatial information of the acoustic wave still remains unclear because a single-frequency continuous probe wave was used in the previous characterization. By either linearly sweeping the probe light frequency (optical frequency domain reflectometry, OFDR) [32,33] or using the pulsed probe light (optical time domain reflectometry, OTDR) [34,35], the distributed spatial information can be obtained, which provides a visual picture of acoustic wave evolution in the spatial domain for us to further understand the acoustic wave noise properties. The requirement of the frequency sweeping in the OFDR technique usually takes a long time, thus hindering its dynamic applications (up to kilohertz) in the distributed sensing. By sending a series of probe pulses and measuring the time-resolved traces in the oscilloscope, OTDR is a good technique for the distributed static and dynamic detection of the acoustic wave in Brillouin random fiber lasers.

In this paper, the acoustic wave in a Brillouin gain fiber generated by a Brillouin random fiber laser (BRFL) is measured by the OTDR technique for the first time. A dynamic grating is introduced by the acoustic wave, where its detection is an SBS-enhanced polarization-decoupled four-wave mixing (FWM) process. Based on the measurement time of one detection process, the distributed detection can be divided into static measurement and dynamic measurement. The static measurement characterizes the time-averaged property of the acoustic wave, in which the frequency of the probe light is swept in several minutes. In dynamic measurement, a series of pulsed probe lights with 10 kHz repetition rate at fixed optical frequency under the phase matching condition is launched into the Brillouin gain fiber, and thus the fast change of the acoustic wave intensity is obtained. The static measurement results find that the Brillouin gain of BRFL depletes exponentially along the Brillouin gain fiber. In addition, the Brillouin gain depletes more quickly at the initial part of the Brillouin gain fiber when the photons of the probe light absorb energy from the acoustic wave. The dynamic detection reveals that the noise source of the BRFL first appears at the initial part of the Brillouin gain fiber and the phase noise of the random laser induces the nonlinear change of the interference dark spots in the spatial-time map. The distributed measurement results provide a new perspective to study the performance and noise properties of the BRFL, which enhances our understanding about the fundamental physics behind random fiber lasers.

2. PRINCIPLE OF ACOUSTIC WAVE DETECTION

A. Theoretical Description

The BRFL makes use of stimulated Brillouin scattering as the gain mechanism, where the pump wave and Stokes wave beat together, giving rise to density variation associated with an acoustic wave through electrostriction effect. The acoustic wave introduces a moving periodically modulated refractive index acting like a moving fiber Bragg grating (FBG) which reflects light at its central wavelength. In the polarization-maintaining (PM) fiber, the property of the moving grating could be detected by monitoring the reflected wave from a probe wave with orthogonal polarization when the phase matching condition is satisfied [36,37]. The detection of the moving dynamic grating is a polarization-decoupled FWM process [38]. The basic configuration of a BRFL is shown in Fig. 1. The pump laser with linear polarization is injected into the slow axis of the Brillouin gain fiber, and the backward Stokes light experiences the distributed Rayleigh scattering along the 500 m PM fiber, providing feedback for the BRFL's radiation. The probe light can be launched into the Brillouin gain fiber either from the initial end or the tail end. In both cases, the pump wave propagates along the $+z$ direction and Stokes wave propagates along the $-z$ direction with the same polarization state along the slow axis, so that the acoustic wave induced by SBS is propagating along the $+z$ direction. When the probe light is launched from the initial end of the Brillouin gain fiber, the probe wave in y polarization has the same propagation direction as the acoustic wave, and thus a reflected wave, whose frequency is downshifted from the

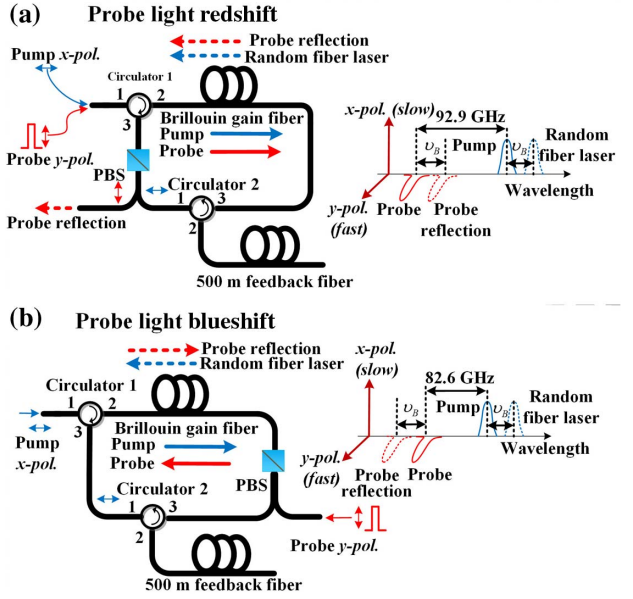

Fig. 1. Configuration of the BRFL and the operation principle of acoustic wave detection when (a) the probe light co-propagates with the acoustic wave and (b) the probe light counter-propagates with the acoustic wave.

frequency of the probe wave by an amount of one Brillouin frequency, experiences a photon energy downconversion process, as shown in Fig. 1(a). On the other hand, if the probe light is launched from the tail end of the Brillouin gain fiber, the probe wave in y polarization has opposite propagation direction to the acoustic wave, and the reflected wave experiences a photon energy upconversion process whose frequency is upshifted from the frequency of the probe wave, as shown in Fig. 1(b). The interactions among the pump wave, Stokes wave, probe wave, and reflected wave are coupled by the dynamic density variation of the Brillouin gain fiber under the phase matching condition, which could be considered as a polarization-decoupled FWM process. The detailed derivation of the four coupled wave can be seen in Ref. [38]. The SBS-induced birefringence change of the Brillouin gain fiber in the polarization-decoupled FWM process can be expressed as [38]

$$\Delta B_{\mathrm{SBS}} = \frac{4\pi n_x \Delta \upsilon_{\mathrm{SBS}}}{\omega_s}, \tag{1}$$

where n_x is the refractive index in the slow axis, ω_s is the optical frequency of Stokes light, and $\Delta \upsilon_{\mathrm{SBS}} = (\upsilon_p - \upsilon_{\mathrm{pr}})_{\text{with SBS}} - (\upsilon_p - \upsilon_{\mathrm{pr}})_{\text{without SBS}}$ is the change of frequency difference between the pump wave and the probe wave induced by the SBS process. Therefore, the SBS-induced birefringence change can be obtained by measuring the value of $\Delta \upsilon_{\mathrm{SBS}}$ in the experiment.

B. Experimental Setup

The experimental setups are mainly composed of three parts: pump and probe light generation part (part A), BRFL configuration part (part B), and reflected light detection part (part C). Figure 2(a) shows the acoustic wave detection setup when the probe light propagates in the same direction with the pump light and acoustic wave. Both the pump light and probe light are generated from a single-frequency laser with 0.1 kHz linewidth in order to make sure that the frequency difference between the pump light and the probe light can be precisely controlled. When the probe light propagates in the same direction with the pump light, photons of the probe light experience the energy downconversion process. In this process, the frequency of the probe light in the fast axis should be 92.9 GHz away from the pump light in the slow axis to make the frequency of the probe light be aligned to the central reflection bandwidth of the dynamic grating. The 92.9 GHz frequency

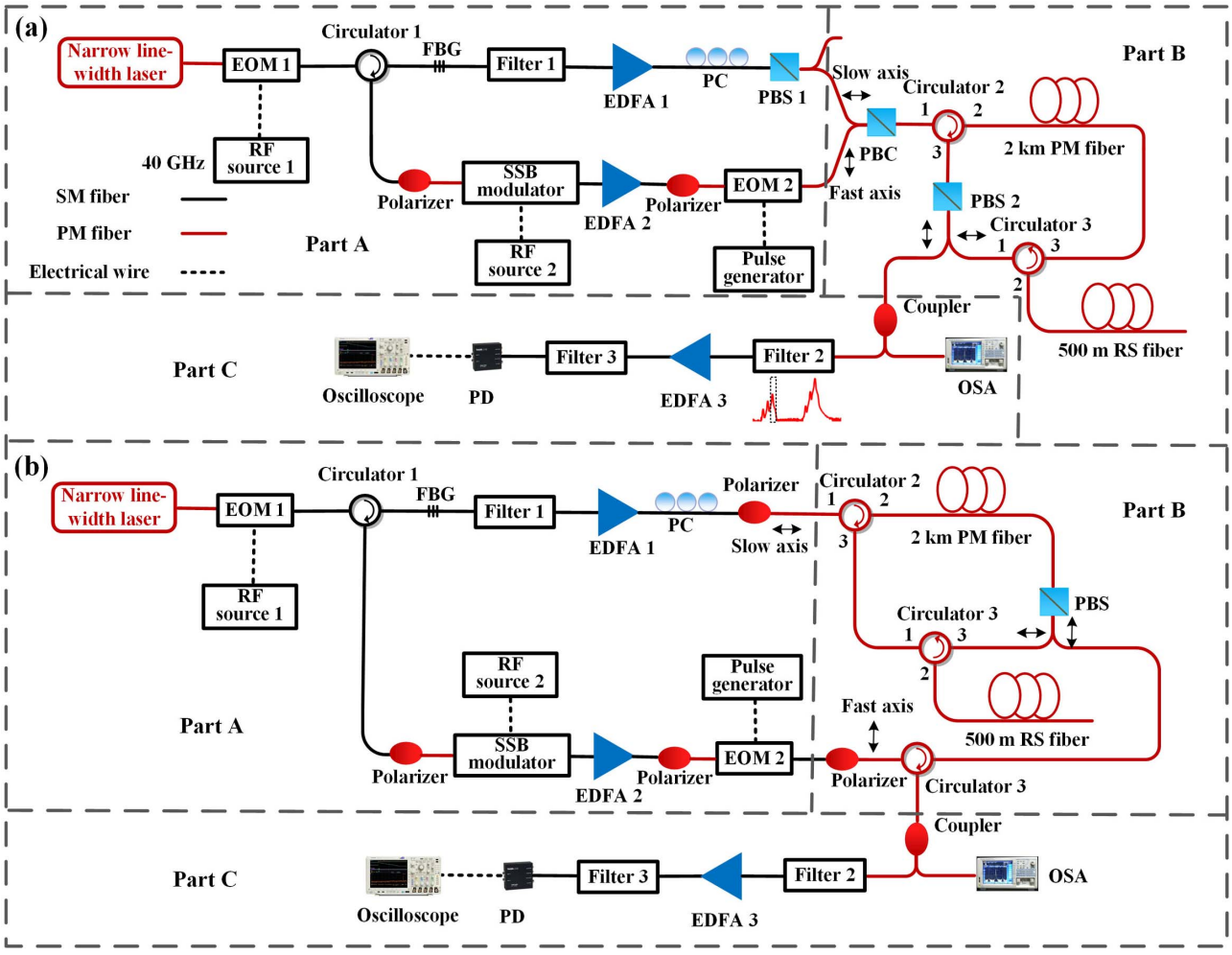

Fig. 2. Configuration of the BRFL and the operation principle of acoustic wave detection when (a) the probe light co-propagates with the acoustic wave and (b) the probe light counter-propagates with the acoustic wave.

separation is determined by the birefringence of the Brillouin gain fiber in the setup. The large frequency separation between the pump light and the probe light is obtained by using a 40 GHz bandwidth electric-optic modulator (EOM 1) combined with a 20 GHz single-sideband (SSB) modulator. First, two light sidebands with 80 GHz separation are generated after the narrow linewidth laser is modulated by EOM 1. Then, the two sidebands are injected to a circulator and a 3 GHz bandwidth FBG, after which one of the sidebands is reflected back by the FBG and the other sideband passes through a 3 GHz bandwidth optical filter to reject light with other optical frequencies. The light after filter 1 is the pump source for the BRFL, which is then amplified by the erbium-doped fiber amplifier 1 (EDFA 1). After EDFA 1, a polarization controller combined with the polarization beam splitter 1 (PBS 1) is used to align polarization of the pump light to the slow axis of the PM fiber. Before being modulated by the SSB modulator, the light from EOM 1 is reflected back by the 3 GHz bandwidth FBG and then passes through circulator 1. A polarizer before the SSB modulator is used to ensure the single polarization state of the light. The frequency of light is shifted 12.9 GHz away by the SSB modulator, after which it is amplified by EDFA 2 and then modulated by EOM 2 to generate 10 ns pulses with 10 kHz repetition rate. The polarizer before EOM 2 is employed to optimize the pulse extinction ratio, which is important to reject noise during the distributed acoustic wave detection process. The pulse after EOM 2 has single polarization state and is aligned to the fast axis of the PM fiber, which is the probe light in the setup. The pump light and probe light are combined together by a polarization beam combiner and then injected to the Brillouin gain fiber of the BRFL through circulator 2. SBS is initiated by the pump light in the Brillouin gain fiber, which is a 2 km long Panda-type PM fiber with a fiber loss of 0.296 dB/km and a mode field diameter of 6.48 μm at the wavelength of 1550 nm. In the slow axis, the backward Stokes light passes through PBS 2 and the 500 m PM Rayleigh scattering (RS) fiber. The backscattered light from the 500 m RS fiber is then injected back to the Brillouin gain fiber to provide distributed feedback for the BRFL. In the fast axis, the probe light is reflected by the co-propagating dynamic grating and experiences an optical frequency redshift. The frequency redshifted probe light then passes through circulator 1 and PBS 2. After PBS 2, the light is split by a coupler, after which one of the paths is directly connected to an optical spectrum analyzer (OSA) to measure its spectrum property, and the other path passes through filter 2 with 3 GHz bandwidth to select the frequency redshifted probe light, which is then amplified by EDFA 3 and detected by a photodetector (PD) and an oscilloscope. Filter 3 after EDFA 3 is used to reject the spontaneous emission from EDFA 3 in order to further reject noise. For the probe light photon energy upconversion process, the probe light propagates in the opposite direction to the acoustic wave and pump light. The experimental setup for the probe light photon energy upconversion process in Fig. 2(b) is similar to the photon energy downconversion process in Fig. 2(a) except that the probe light is injected to the other end of the 2 km long Brillouin gain fiber in Fig. 2(b). The frequency separation between pump light and probe light is decreased to 82.5 GHz in the probe light photon energy upconversion process, which is the subtraction of 92.9 GHz and 10.4 GHz (Brillouin frequency shift of the 2 km long PM fiber).

3. RESULTS

A. Distributed Static Measurement of Gain Profile

After the pulsed probe light is launched into the Brillouin gain fiber, it is reflected by the dynamic grating which is induced by the refractive index modulation of the acoustic wave. Figure 3(a) shows the spectrum measured on the OSA. When the pump laser is off, the probe light is reflected by Rayleigh scattering and its spontaneous Brillouin scattering [blue curve in Fig. 3(a)]. After the pump laser is turned on, most of the reflected probe light would experience a redshift [red curve in Fig. 3(a)]. The reflected light is detected by the PD and oscilloscope, where the time-resolved traces on the oscilloscope show the reflected light intensity distribution in the spatial domain. By sweeping the optical frequency difference between the pump light and probe light, the distributed reflection spectra of the dynamic grating can be obtained. Figure 3(b) shows the three-dimensional reflected light intensity in the spatial domain at different optical frequency separation between the pump light and probe light. The fitting dynamic grating spectral width is around 100 MHz, which results from the convolution of the probe pulse spectra and the intrinsic dynamic grating spectra, and thus a longer probe pulse can give a narrower spectrum and a better frequency and birefringence accuracy at the expense of sacrificing the spatial resolution. The reflectivity of the dynamic grating is determined by the refractive index modulation depth (intensity of the acoustic wave) of the fiber,

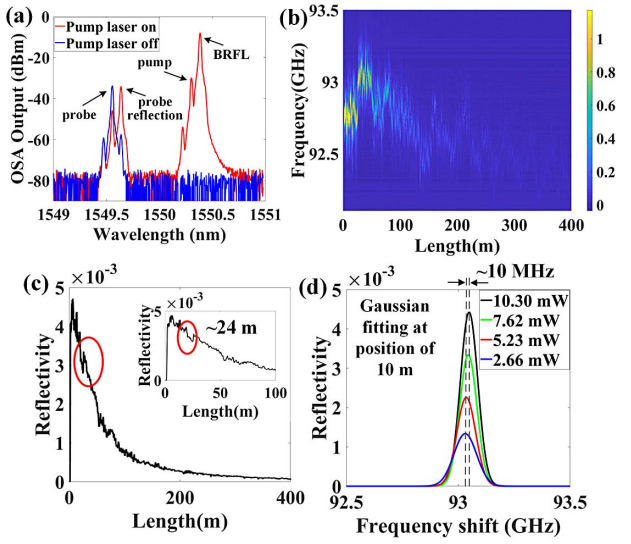

Fig. 3. (a) Spectrum measured on the OSA when the pump laser is turned on (red) and turned off (blue). (b) Distributed reflection spectra of the dynamic grating induced by the acoustic wave in the BRFL for the probe light photon energy downconversion process. (c) Reflectivity of the dynamic grating in the spatial domain along the Brillouin gain fiber. (d) Gaussian fitting of the reflection spectra of the dynamic grating at position of 10 m at maximum gain when the output powers of the BRFL are 10.3 mW, 7.62 mW, 5.23 mW, and 2.66 mW, respectively.

which is proportional to the Brillouin gain of the BRFL. This provides a direct distributed gain profile measurement method of the BRFL in the spatial domain. The averaged reflectivity of the dynamic grating can be obtained by integrating the dynamic grating spectra in the frequency domain of Fig. 3(b). As shown in Fig. 3(c), the reflectivity of the dynamic grating decreases exponentially in the spatial domain, indicating that the gain of the BRFL decreases exponentially in the spatial domain due to the pump depletion. After the position of 400 m, almost all of the pump light is converted to its Stokes light and the Brillouin gain nearly drops to zero. At some particular position, such as the position around 24 m, the Brillouin gain is slightly deviated from the exponential curve due to the relatively large birefringence fluctuation at those positions, as can be seen in Fig. 3(b). This is because the linewidth of the BRFL is of the order of subkilohertz, which is much narrower than the Brillouin gain bandwidth. Any tiny birefringence fluctuation of the Brillouin gain fiber can lead to the frequency change of the BRFL. The BRFLs have optimized gain at the position where the central frequency of the Brillouin gain spectrum is aligned to the operation optical frequency of the BRFL, while at other positions the Brillouin gain is decreased due to the misalignment of the local Brillouin gain spectra with the operation optical frequency of the BRFL. The misalignment between the local Brillouin gain spectra and the operation optical frequency of the BRFL is one of the noise sources for the mode hopping and laser intensity fluctuation. At the initial 10 m of the Brillouin gain fiber, the spectra of the dynamic grating show slight central frequency variation at different operation powers of the BRFL due to the SBS random laser-induced birefringence change of the fiber. For example, Fig. 3(d) shows that, at the position of 10 m, the maximum central frequency change of the dynamic grating spectra is of the order of 10 MHz, corresponding to 10^{-7} birefringence change of the PM fiber according to Eq. (1). Beyond the initial 10 m, the birefringence of the fiber induced by the random fiber laser is too small to be detected due to the pump power depletion. The average power of the probe light is around 0.25 mW. The power of the pump light is above 40 mW to generate the random laser radiation. The probe power is relatively weak compared to the pump power to ensure the minimum disturbance to the BRFL.

There is a problem using the probe light photon energy downconversion process to detect the acoustic wave in the BRFL. Since the refractive index modulation depth of the dynamic grating at the beginning of the Brillouin gain fiber is much stronger than in the latter part, it is hard to know whether the power of the probe light is depleted or not at the beginning of the Brillouin gain fiber. To verify this point, the probe light is launched to the Brillouin gain fiber from the opposite direction to the propagating direction of the pump light. In this detection mechanism, the reflected probe light experiences an optical frequency blueshift instead of redshift because of the counter-propagating direction between the acoustic wave and the probe light. Figure 4(a) shows the spectra measured on the OSA when the optical frequency of the probe light is aligned or misaligned to the central wavelength of the dynamic grating, respectively. When the optical frequency of

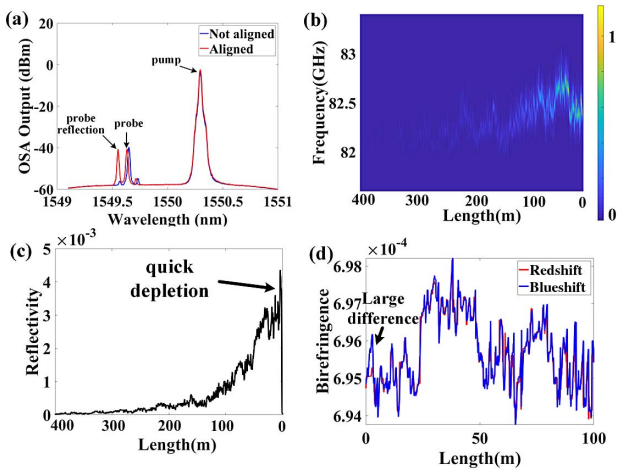

Fig. 4. (a) Spectrum of the reflected probe light measured on the OSA for the probe light photon energy upconversion process. (b) Distributed reflection spectra of the dynamic grating induced by the acoustic wave in the BRFL. (c) Reflectivity of the dynamic grating in the spatial domain along the Brillouin gain fiber. (d) Birefringence of the Brillouin gain fiber measured by the optical frequency redshifted probe light and optical frequency blueshifted probe light.

the probe light is aligned to the central wavelength of the dynamic grating, the blueshifted reflected light can be detected by the OSA. Otherwise, there is no reflection of the probe light. The three-dimensional distributed dynamic grating spectra in the spatial domain is plotted in Fig. 4(b). Because of the quick depletion of pump light in the Brillouin gain fiber, the reflection of the probe light can only be detected at the first 400 m part after the pump light is launched to the Brillouin gain fiber. Therefore, only the initial 400 m part near the pump injection with the highest Brillouin gain is plotted in Fig. 4(b). Similar to Fig. 3(b), the central frequency of the dynamic grating spectra, which is determined by the birefringence of the PM fiber, characterizes the distributed birefringence of the Brillouin gain fiber. Because the probe light is injected from the other end of the Brillouin gain fiber, the distributed birefringence measurement result in Fig. 4(b) is the inverse of the distributed birefringence value in Fig. 3(b) in the spatial domain. The reflectivity of the dynamic grating, which is proportional to the local Brillouin gain, is also obtained by integrating the dynamic grating spectra in the frequency domain of Fig. 4(b). Figure 4(c) shows that the overall trend of the distributed Brillouin gain exhibits an exponential increase in the spatial domain, which confirms the exponential decrease of the Brillouin gain measured by the probe light photon energy downconversion process. The results manifest that the probe light in the photon energy downconversion process is not depleted because of the weak reflectivity of the dynamic grating. The weak reflectance of the dynamic grating is caused by the nonuniform birefringence of the Brillouin gain fiber, leading to the result that the central reflection spectrum of the dynamic grating written by the acoustic wave is not perfectly aligned to the optical frequency of the probe light at most positions of the Brillouin gain fiber. For the probe light photon energy

upconversion process, the pump light is depleted more quickly than the probe light photon energy downconversion process at the initial part of the Brillouin gain fiber. This is because in the photon energy upconversion process, the photons of the probe light absorb energy from the acoustic phonons and pump light photons, which makes them depleted more quickly in the spatial domain. The quick depletion of pump light makes the gain of the BRFL focus at the initial part of the Brillouin gain fiber, leading to a large birefringence change at the highest gain part of the Brillouin gain fiber. Figure 4(d) compares the distributed birefringence of the Brillouin gain fiber measured by redshifted probe light and blueshifted probe light, respectively. It can be seen that at the initial part of the Brillion gain fiber, the birefringence detected by the blueshifted probe light deviates approximately 10^{-6} from the birefringence detected by the redshifted probe light. At the rest of the positions, the birefringence measured by the two mechanisms agrees with each other well. This confirms the quick Brillouin gain depletion at the initial part of the Brillouin gain fiber in Fig. 4(c), proving that the focusing of the high gain leads to large birefringence change of the Brillouin gain fiber.

B. Distributed Dynamic Measurement of Gain Profile

The dynamic gain profile measurement is implemented by sending a series of probe pulses at a repetition rate of 10 kHz to measure the distributed intensity of the acoustic wave in the BRFL. These results are also plotted in three-dimensional figures where the x axis represents the position and the y axis represents the time, as shown in Figs. 5(a) and 5(b). The distributed dynamic gain profile of the BRFL provides information on the dynamic process of mode hopping and mode competition in the BRFL. The interference fringes of the BRFL in the Brillouin gain fiber in the spatial domain and in the time domain can be observed simultaneously. At a fixed position, the intensity of the acoustic wave fluctuates periodically in the time domain which is caused by mode hopping. Because the BRFL is easily disturbed by the environmental perturbation [17], the Brillouin gain profile and the feedback provided by the Rayleigh scattering are not ultra-stable. The operating mode of the BRFL switches from one frequency to other frequencies from time to time due to the random mode competition in the BRFL, which is the origin of mode hopping in the BRFL. By measuring the distributed dynamic gain profile, the interference fringes of the Stokes light in the spatial domain are also obtained at a fixed time. The fringe patterns measured by the pulsed probe light for the photon energy upconversion process and the photon energy downconversion process exhibit different characteristics in the spatial domain. For the photon energy upconversion process in Fig. 5(b), the pulsed probe light propagates in the same direction and velocity as the beat pattern. For example, if the peak of the beat signal is detected by the probe light at time T_1, the pulsed probe light would propagate together with the same peak along the Brillouin gain fiber at time T_2 and time T_3, as shown in Fig. 5(d). The OTDR technique uses the time-resolved trace to discriminate the backscattered light at different positions in a fiber. This explains why the dark spot (or bright spot) of the interference fringes in Fig. 5(b) always appears at all of the positions along the Brillouin gain fiber at a fixed time. The

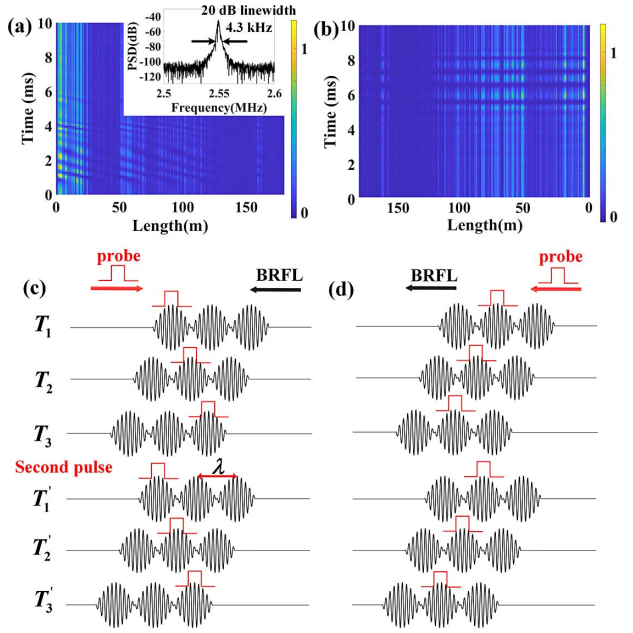

Fig. 5. (a) Spatial-time map of the acoustic wave intensity when the probe light experiences the photon energy downconversion process. The inset figure is the spectrum measurement of two beating modes when mode hopping occurs in the BRFL. (b) The spatial-time map of the acoustic wave intensity when the probe light experiences the photon energy upconversion process. (c) Schematic diagram of the acoustic wave detection process when the probe light experiences the photon energy downconversion process. (d) Schematic diagram of the acoustic wave detection process when the probe light experiences the photon energy upconversion process.

phenomenon proves that the mode hopping beat pattern co-propagates with the Stokes light in the Brillouin gain fiber during the random mode switching process. In contrast, when the probe light counter-propagates with the Stokes light, a single pulse can detect all of the peaks of the beat pattern that are transmitted in the Brillouin gain fiber. For example, if a peak of the beat signal is detected by the probe light at time T_1, the following two peaks can also be detected by the probe light in sequence at time T_2 and T_3, as shown in Figs. 5(a) and 5(c). This provides us with a method to study how the fringes evolve dynamically in the spatial domain. In Fig. 5(a), the dynamic distributed acoustic wave measurement shows that the fringes always first appear at the initial position of the Brillouin gain fiber. The initial position means the fiber end where the pump light is first launched to the Brillouin gain fiber. The interference fringes are the envelope of the beat signal between different random modes of the BRFL. If there is only one dominant lasing mode, no interference fringe can be detected. When the gain of the light inside the random cavity is greater than the loss at other frequencies, other random modes start to compete with the original dominant random modes in the Brillion gain fiber with limited Brillouin gain. As the initial part of the Brillouin gain fiber has the highest gain, it is also the place where the condition that the gain is greater than the loss can be first satisfied. The dark spot of the fringes measured by the pulsed probe light moves along the Brillouin gain fiber. However,

the slope of these dark lines in Fig. 5(a) does not represent the real moving velocity of the beat pattern. As shown in Fig. 5(c), the time difference between two consecutive pulses is $\Delta T = T_1' - T_1$. During this time interval, the displacement of the light is $(T_1' - T_1)c/n$ and N periods of the beat pattern have passed the same position on the Brillouin gain fiber. N is the integer of $(T_1' - T_1)c/n\lambda$, and the slope of the dark lines in Fig. 5(c) can be expressed as $k = c/n - N\lambda/\Delta T$, where the λ is the wavelength of the envelope. With the fixed pulse repetition rate, the slope of the dark lines is determined by the envelope of the beat pattern since the fixed pulse repetition rate is used. Therefore, the constant linear slope of these dark lines represents zero phase noise in the beat pattern. Longer duration time of the linear dark lines represents smaller detected linewidth of the BRFL. The minimum detected 20 dB linewidth of the BRFL in the experiment is 4.3 kHz, which is measured by Fourier transform of the output intensity of the BRFL when the beat pattern occurs, as shown in the inset curve in Fig. 5(a). The phase noise of the beat pattern leads to nonlinear slope changes of the dark lines in Fig. 5(a), which is caused by the frequency change of the BRFL and nonlinear group index change induced by the acoustic wave. Due to the Kramers–Kronig relation, changes in the gain or loss of a medium are always accompanied with changes in the refractive index. Although the magnitude of the refractive index changes is relatively small, it varies rapidly with the frequency of Stokes light near the Brillouin gain peak [36]. Because the velocity of the beat pattern is the group velocity of the envelop related to $\Delta\omega/\Delta k$, rapid changes of the refractive index can change the group index considerably and affect the group velocity of the beat pattern. The distributed interference fringes measured by detecting the dynamic grating through pulsed probe light provide us with a new method to study the phase noise of the BRFL, which could help us to better understand the random nature of the BRFL and to further improve its performance in practical applications.

The peak amplitude of the acoustic wave intensity fluctuation in one second is counted for the two detection mechanisms. Figures 6(a) and 6(b) show its statistical distribution histograms at high gain position and low gain position, respectively, when the BRFL is near the lasing threshold. The high gain position part refers to the position of the first 10 m of the Brillouin gain fiber and the low gain position refers to the position of 310 m to 320 m of the Brillouin gain fiber. Near the lasing threshold, the L-shaped long-tailed histograms characteristic of extreme value behavior are observed at both the high gain position and the low gain position. The x axis in Fig. 6 is normalized by the corresponding significant wave height (SWH), which is defined as the mean height of the highest third of the acoustic wave intensity [39]. The event of the peak amplitude more than twice the SWH can be considered as a rogue (extreme) event. Therefore, the generation of optical rogue wave (RW) is detected in the BRFL near the lasing threshold. Moreover, at the high gain position in Fig. 6(a), the highest recorded peak intensity reaches about 6 times that of the corresponding SWH, and the occurrence proportion of RW events is about 14%. At the low gain position in Fig. 6(b), the highest peak intensity is only about 4 times that of the corresponding SWH, and the generation probability of the RW decreases to 5.6%. The underlying physics for the RW generation is that the SBS process is initiated from the thermal noises in the fiber. The temporal output is a mixture of amplified noisy Stokes light and lasing Stokes light, depending on whether or not the stochastic lasing occurs [40]. The amplification of the thermal noise in the BRFL is similar to the modulation instability seeded from noise that results in a series of high-contrast peaks of random intensity [39,41]. The higher proportion of the RW events at the high gain position than

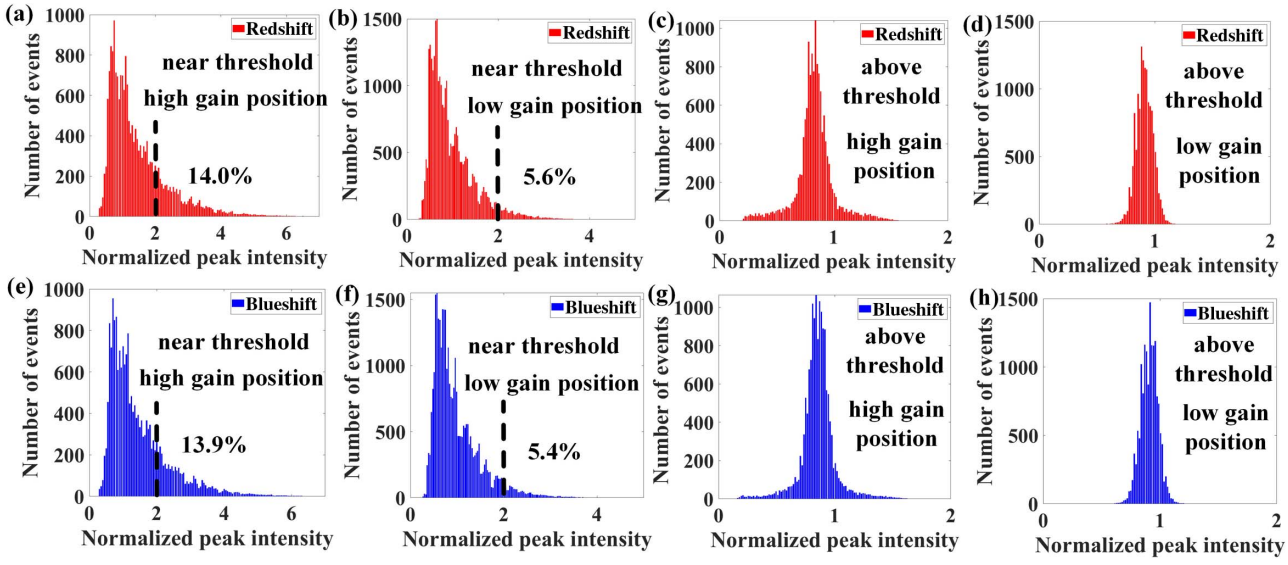

Fig. 6. Histograms of the temporal intensity statistical distribution near the lasing threshold at (a) high gain position and (b) low gain position for redshifted probe light measurement. Histograms of the temporal intensity statistical distribution above the lasing threshold at (c) high gain position and (d) low gain position for redshifted probe light measurement. Histograms of the temporal intensity statistical distribution near the lasing threshold at (e) high gain position and (f) low gain position for blueshifted probe light measurement. Histograms of the temporal intensity statistical distribution above the lasing threshold at (c) high gain position and (d) low gain position for blueshifted probe light measurement.

at the low gain position indicates that the random intensity initiated from thermal noise is amplified nonlinearly on the Brillouin gain fiber. The SBS dynamics can be described by the amplitude coupled equations among the pump wave, Stokes wave, and probe wave [36,42,43], where higher peak density variation of the acoustic wave leads to higher wave coupling between the pump wave and the Stokes wave. The nonlinear transfer function of the SBS process modifies the temporal intensity probability distribution of the mixing noisy Stokes light and lasing Stokes light, leading to a higher proportion of the RW events at the high gain position of the Brillouin gain fiber. When the BRFL is far above the lasing threshold, the temporal statistical distribution histograms at the high gain position and low gain position show a Gaussian distribution because of the stable establishment of the BRFL emission above the lasing threshold. Because the highly coherent BRFL and acoustic phonons are established, the thermal noise is rejected and the optical RW cannot be detected anymore as there are no events of the peak amplitude more than twice the SWH, as shown in Figs. 6(c) and 6(d). However, the temporal intensity at the high gain position exhibits more events with high peak intensity fluctuation than that of temporal intensity at the low gain position when the BRFL is above the lasing threshold, which is mainly attributed to the following two reasons. First, the nonlinear transfer function of the SBS process combined with the inhomogeneous gain in the spatial domain amplifies intensity fluctuation nonlinearly. Therefore, a small signal fluctuation at the position with low gain could lead to tremendous peak intensity fluctuation at the position with high gain. At the same time, intensity fluctuations are continuously introduced into the laser dynamics during the laser amplification process along the Brillouin gain fiber. The peak fluctuations at the high gain position are accumulated from multiple intensity fluctuations on the Brillouin gain fiber, which is the origin of the relative high peak fluctuation. Second, the nonuniform birefringence [as shown in Fig. 4(d)] of the Brillouin gain fiber corresponds to nonuniform gain spectra in the spatial domain, creating various localized gain areas since the optical frequency linewidth of the BRFL is ultra-narrow. Because the localized gain area at the high gain position obtains high energy due to the mode competition with limited total Brillouin gain, it is also the place where the mode competition is fiercest, thus inducing a relatively high peak intensity fluctuation when mode competition happens. Since a small amplitude signal at the low gain position of the Brillouin gain fiber can be dramatically amplified at the high gain position, the low gain position of the fiber is more sensitive to small signal variation. For instance, Fig. 6(d) has smaller intensity fluctuation at the low gain region, however Fig. 6(c) represents larger intensity variation. Having higher gain is not equivalent to lower intensity noise for the same pump power; such a distributed spatial gain distribution illustrates that relatively lower gain gives more stable power in random SBS laser, which allows higher sensitivity sensing. The ability of small signal amplification on the Brillouin gain fiber could potentially improve the sensitivity of the distributed sensor based on the BRFL. Figures 6(a)–6(d) are the results when the probe light co-propagates with the acoustic wave and experiences an optical frequency redshift, while Figs. 6(e)–6(h) are the results when the probe light counter-propagates with the acoustic wave and experiences an optical frequency blueshift. The blueshifted probe light measurement results agree with the redshifted probe light measurement results, which confirms the optical RW detection result of the BRFL.

4. CONCLUSION

The distributed detection of the acoustic wave generated by the BRFL is realized based on the OTDR technique for the first time. The detection is an SBS-enhanced polarization-decoupled FWM process where the probe light experiences maximum reflection when phase matching condition is satisfied. Photons of the probe light can either give energy to the acoustic phonons or absorb energy from the acoustic phonons, depending on the relative propagation direction of the acoustic wave and the probe light. In the static measurement, the distributed dynamic grating spectra are obtained by sweeping the frequency of the probe light. The Brillouin gain depletes exponentially along the Brillouin gain fiber in the BRFL. When the photons of the probe light absorb energy from the acoustic wave, a quick depletion of the Brillouin gain is observed in the experiment. The SBS-induced birefringence variations are estimated to be approximately 10^{-7} to 10^{-6} by measuring the central frequency change of the dynamic grating spectra. In the dynamic measurements, the intensity noise of the laser is found to first occur at the highest gain position of the Brillouin gain fiber. The phase noise of the BRFL leads to wavelength variation of the beat pattern, which further leads to nonlinear dark spot change in the spatial-time acoustic wave intensity map. The spatial-time acoustic wave intensity map provides a new method to characterize the phase noise of the BRFL and to study its dynamic evolution process. Optical RWs are found near the lasing threshold of the BRFL, where the nonlinear transfer function of the SBS process modifies the temporal intensity probability distribution of the mixing noisy Stokes light and lasing Stokes light. Above the lasing threshold, the temporal intensity at the high gain position exhibits more events with high peak intensity fluctuation than the temporal intensity at the low gain position, which is caused by the SBS nonlinear transfer function and the localized gain in the BRFL. The detection results enhance our understanding on the BRFL, paving the way for its performance improvement in future applications in the fields of communication, high-precision metrology, sensing, and spectroscopy.

Funding. Canada Research Chairs (950231352); Natural Sciences and Engineering Research Council of Canada (RGPIN-2020-06302).

Disclosures. The authors declare no conflicts of interest.

REFERENCES

1. S. K. Turitsyn, S. A. Babin, A. E. El-Taher, P. Harper, D. V. Churkin, S. I. Kablukov, J. D. Ania-Castañón, V. Karalekas, and E. V. Podivilov, "Random distributed feedback fibre laser," Nat. Photonics **4**, 231–235 (2010).
2. A. A. Fotiadi, "An incoherent fibre laser," Nat. Photonics **4**, 204–205 (2010).

3. S. K. Turitsyn, S. A. Babin, D. V. Churkin, I. D. Vatnik, M. Nikulin, and E. V. Podivilov, "Random distributed feedback fibre lasers," Phys. Rep. **542**, 133–193 (2014).
4. D. V. Churkin, S. Sugavanam, I. D. Vatnik, Z. Wang, E. V. Podivilov, S. A. Babin, Y. Rao, and S. K. Turitsyn, "Recent advances in fundamentals and applications of random fiber lasers," Adv. Opt. Photonics **7**, 516–569 (2015).
5. M. Skvortsov, S. Abdullina, A. Wolf, A. Dostovalov, A. Vlasov, I. Lobach, S. Wabnitz, and S. Babin, "Random Raman fiber laser based on a twin-core fiber with FBGs inscribed by femtosecond radiation," Opt. Lett. **44**, 295–298 (2019).
6. C. J. de Matos, L. D. S. Menezes, A. M. Brito-Silva, M. M. Gámez, A. S. Gomes, and C. B. de Araujo, "Random fiber laser," Phys. Rev. Lett. **99**, 153903 (2007).
7. Z. Hu, Q. Zhang, B. Miao, Q. Fu, G. Zou, Y. Chen, Y. Luo, D. Zhang, P. Wang, H. Ming, and Q. Zhang, "Coherent random fiber laser based on nanoparticles scattering in the extremely weakly scattering regime," Phys. Rev. Lett. **109**, 253901 (2012).
8. I. R. R. Gonzalez, B. C. Lima, P. I. Pincheira, A. A. Brum, A. M. Macedo, G. L. Vasconcelos, L. D. S. Menezes, E. P. Raposo, A. S. Gomes, and R. Kashyap, "Turbulence hierarchy in a random fibre laser," Nat. Commun. **8**, 15731 (2017).
9. E. Turitsyna, S. Smirnov, S. Sugavanam, N. Tarasov, X. Shu, S. Babin, E. Podivilov, D. Churkin, G. Falkovich, and S. Turitsyn, "The laminar–turbulent transition in a fibre laser," Nat. Photonics **7**, 783–786 (2013).
10. A. S. Gomes, B. C. Lima, P. I. Pincheira, A. L. Moura, M. Gagné, E. P. Raposo, C. B. de Araújo, and R. Kashyap, "Glassy behavior in a one-dimensional continuous-wave erbium-doped random fiber laser," Phys. Rev. A **94**, 011801 (2016).
11. B. C. Lima, P. I. Pincheira, E. P. Raposo, L. D. S. Menezes, C. B. de Araújo, A. S. Gomes, and R. Kashyap, "Extreme-value statistics of intensities in a CW-pumped random fiber laser," Phys. Rev. A **96**, 013834 (2017).
12. J. Li, H. Wu, Z. Wang, S. Lin, C. Lu, E. P. Raposo, A. S. Gomes, and Y. Rao, "Lévy spectral intensity statistics in a Raman random fiber laser," Opt. Lett. **44**, 2799–2802 (2019).
13. Y. Xu, L. Zhang, S. Gao, P. Lu, S. Mihailov, and X. Bao, "Highly sensitive fiber random-grating-based random laser sensor for ultrasound detection," Opt. Lett. **42**, 1353–1356 (2017).
14. Z. Wang, Y. Rao, H. Wu, P. Li, Y. Jiang, X. Jia, and W. Zhang, "Long-distance fiber-optic point-sensing systems based on random fiber lasers," Opt. Express **20**, 17695–17700 (2012).
15. D. Leandro, V. deMiguel Soto, R. A. Perez-Herrera, M. B. Acha, and M. López-Amo, "Random DFB fiber laser for remote (200 km) sensor monitoring using hybrid WDM/TDM," J. Lightwave Technol. **34**, 4430–4436 (2016).
16. Y. Xu, S. Gao, P. Lu, S. Mihailov, L. Chen, and X. Bao, "Low-noise Brillouin random fiber laser with a random grating-based resonator," Opt. Lett. **41**, 3197–3200 (2016).
17. Y. Li, P. Lu, F. Baset, Z. Ou, J. Song, A. Alshehri, V. R. Bhardwaj, and X. Bao, "Narrow linewidth low frequency noise Er-doped fiber ring laser based on femtosecond laser induced random feedback," Appl. Phys. Lett. **105**, 101105 (2014).
18. M. Pang, X. Bao, L. Chen, Z. Qin, Y. Lu, and P. Lu, "Frequency stabilized coherent Brillouin random fiber laser: theory and experiments," Opt. Express **21**, 27155–27168 (2013).
19. Z. Zhou, P. Lu, L. Zhang, S. Mihailov, L. Chen, and X. Bao, "Thermal and acoustic noise insensitive Brillouin random fiber laser based on polarization-maintaining random fiber grating," Opt. Lett. **44**, 4195–4198 (2019).
20. O. A. Gorbunov, S. Sugavanam, and D. V. Churkin, "Intensity dynamics and statistical properties of random distributed feedback fiber laser," Opt. Lett. **40**, 1783–1786 (2015).
21. O. Gorbunov, S. Sugavanam, I. Vatnik, and D. Churkin, "Statistical properties of radiation of multiwavelength random DFB fiber laser," Opt. Express **24**, 19417–19423 (2016).
22. D. V. Churkin, I. V. Kolokolov, E. V. Podivilov, I. D. Vatnik, M. A. Nikulin, S. S. Vergeles, I. S. Terekhov, V. V. Lebedev, G. Falkovich, S. A. Babin, and S. K. Turitsyn, "Wave kinetics of random fibre lasers," Nat. Commun. **6**, 6214 (2015).
23. B. C. Lima, A. S. Gomes, P. I. Pincheira, A. L. Moura, M. Gagné, E. P. Raposo, C. B. de Araújo, and R. Kashyap, "Observation of Lévy statistics in one-dimensional erbium-based random fiber laser," J. Opt. Soc. Am. B **34**, 293–299 (2017).
24. E. Raposo and A. Gomes, "Analytical solution for the Lévy-like steady-state distribution of intensities in random lasers," Phys. Rev. A **91**, 043827 (2015).
25. S. Sugavanam, M. Sorokina, and D. V. Churkin, "Spectral correlations in a random distributed feedback fibre laser," Nat. Commun. **8**, 15514 (2017).
26. A. Klein, G. Masri, H. Duadi, K. Sulimany, O. Lib, H. Steinberg, S. A. Kolpakov, and M. Fridman, "Ultrafast rogue wave patterns in fiber lasers," Optica **5**, 774–778 (2018).
27. J. Xu, J. Wu, J. Ye, J. Song, B. Yao, H. Zhang, J. Leng, W. Zhang, P. Zhou, and Y. Rao, "Optical rogue wave in random fiber laser," Photon. Res. **8**, 1–7 (2020).
28. L. Zhang, Y. Xu, S. Gao, B. Saxena, L. Chen, and X. Bao, "Linearly polarized low-noise Brillouin random fiber laser," Opt. Lett. **42**, 739–742 (2017).
29. M. Pang, X. Bao, and L. Chen, "Observation of narrow linewidth spikes in the coherent Brillouin random fiber laser," Opt. Lett. **38**, 1866–1868 (2013).
30. Z. Zhou, L. Chen, and X. Bao, "Dynamic detection of acoustic wave generated by polarization maintaining Brillouin random fiber laser," APL Photon. **5**, 096101 (2020).
31. I. A. Lobach, R. V. Drobyshev, A. A. Fotiadi, E. V. Podivilov, S. I. Kablukov, and S. A. Babin, "Open-cavity fiber laser with distributed feedback based on externally or self-induced dynamic gratings," Opt. Lett. **42**, 4207–4210 (2017).
32. B. J. Soller, D. K. Gifford, M. S. Wolfe, and M. E. Froggatt, "High resolution optical frequency domain reflectometry for characterization of components and assemblies," Opt. Express **13**, 666–674 (2005).
33. Z. Lou, B. Yang, K. Han, X. Wang, H. Zhang, X. Xi, and Z. Liu, "Real-time *in-situ* distributed fiber core temperature measurement in hundred-watt fiber laser oscillator pumped by 915/976 nm LD sources," Sci. Rep. **10**, 9006 (2020).
34. K. Y. Song, "High-sensitivity optical time-domain reflectometry based on Brillouin dynamic gratings in polarization maintaining fibers," Opt. Express **20**, 27377–27383 (2012).
35. Y. H. Kim and K. Y. Song, "Optical time-domain reflectometry based on a Brillouin dynamic grating in an elliptical-core two-mode fiber," Opt. Lett. **42**, 3036–3039 (2017).
36. R. W. Boyd, *Nonlinear Optics* (Academic, 2020).
37. J. Kim, M. C. Kuzyk, K. Han, H. Wang, and G. Bahl, "Non-reciprocal Brillouin scattering induced transparency," Nat. Phys. **11**, 275–280 (2015).
38. D.-P. Zhou, L. Chen, and X. Bao, "Polarization-decoupled four-wave mixing based on stimulated Brillouin scattering in a polarization-maintaining fiber," J. Opt. Soc. Am. B **30**, 821–828 (2013).
39. J. M. Dudley, F. Dias, M. Erkintalo, and G. Genty, "Instabilities, breathers and rogue waves in optics," Nat. Photonics **8**, 755–764 (2014).
40. Y. Xu, P. Lu, and X. Bao, "Compact single-end pumped Brillouin random fiber laser with enhanced distributed feedback," Opt. Lett. **45**, 4236–4239 (2020).
41. E. J. Kelleher, J. C. Travers, S. V. Popov, and J. R. Taylor, "Role of pump coherence in the evolution of continuous-wave supercontinuum generation initiated by modulation instability," J. Opt. Soc. Am. B **29**, 502–512 (2012).
42. A. A. Fotiadi and R. V. Kiyan, "Cooperative stimulated Brillouin and Rayleigh backscattering process in optical fiber," Opt. Lett. **23**, 1805–1807 (1998).
43. G. P. Agrawal, *Nonlinear Fiber Optics* (Academic, 2013).